POST-BUCKLED PRECOMPRESSED ELEMENTS: A NEW CLASS OF FLIGHT CONTROL ACTUATORS ENHANCING MORPHING WING UAVS

Roelof Vos
Aerospace Engineering Department, The University of Kansas

Keywords: *Adaptive, Piezoelectric, Post-Buckled Precompressed, Morphing*

Abstract

The design, manufacturing and testing of a new class of actuators for morphing wing flight control on subscale Uninhabited Aerial Vehicles (UAVs) is detailed. This class of actuators employed a piezoelectric flight control mechanism which relied on axial precompression to magnify control deflections and control forces simultaneously. A design was made employing these Post-Buckled Precompressed (PBP) bending actuator elements integrated in the outboard wing stations of a 1.4 m span subscale UAV in place of ailerons. The axially compressed actuators were positioned between a tapered D-spar at the 40% chord and a trailing edge stiffener at the 98% chord. Axial precompression in the actuator elements was generated by an elastic skin which covered the outside of the wing and also served as the aerodynamic surface over the aft 70% of the wing chord. Bench tests showed that the axially compressed actuator elements increased deflection by more than 100% compared to conventional piezoelectric bender elements, resulting in a maximum peak-to-peak deflection of the wing of 6.2 deg. Wind tunnel test proved that the section lift coefficient was changed with 8.6% for every degree of wing deflection. Video footage of flight tests demonstrated that with respect to the baseline aircraft, the new PBP equipped aircraft had roughly 38% more roll control authority and the control derivatives were 3.7 times greater. With respect to conventional electromechanical servoactuators, applying PBP actuators led to a saving in operating empty weight by 3.5% and an increase in break frequency from 3Hz up to 34Hz. Moreover, switching to PBP actuators decreased current draw, power consumption, slop and part count with at least an order of magnitude.

Nomenclature

A	in-plane laminate stiffness, N/m
B	Coupled laminate stiffness, N
D	Bending laminate stiffness, Nm
b	Actuator width, m
c	Chord, m
c_l, C_L	Section and wing lift coefficient, $-$
f	Frequency, Hz
F_a	Precompression force, N
K	Structural stiffness, N/m
L	Actuator length, m
M	Applied moment vector, Nm
N	Applied force vector, N

Greek Symbols

α	Angle of attack, deg
δ	PBP local Deflection, deg
δ	Trailing-edge deflection, deg
ε	Normal strain, -
θ	Trailing-edge end rotation, deg
Θ	Normalized Trailing-edge end rotation, $-$
κ	Curvature, $1/deg$
Λ	Unloaded actuator strain, $-$

ρ	Density, kg/m^3
σ	Normal stress, N/m^2

Subscripts

a	Actuator
ex	External
l	Laminate
sp	Negative spring rate
t	Thermal

Abbreviations

CLPT	Classical Laminated Plate Theory
PBP	Post-Buckled Precompressed
PZT	Lead Titanate Zincronate
UAV	Uninhabited Aerial Vehicle

1 Introduction

Conventional roll control on aircraft is achieved by differential aileron deflection. By deflecting a relatively small surface (typically between 10% and 30% of the local wing chord[1]) over a relatively large angle, the aerodynamic loading of the wing is locally changed resulting in a rolling moment. Although effective when properly designed, conventional aileron controls typical consist of hundreds of components and can contribute up to 4% of the aircrafts gross weight.[2]

Adaptive or 'smart' materials have been used successfully in the past decade to enhance aircraft control. Ranging from solid state adaptive rotors and flaps to pitch active wings, all of these concepts have been proven on the bench, in the wind tunnel and eventually in flight.[3–5] In 1996 a solid state adaptive rotor was conceived employing piezoelectric actuators that controlled the blade pitch of the rotor blades resulting in a drop in control system weight by 40% and a drop in power consumption.[6–11] In 2000 an aircraft with active pitch wings controlled by shape memory alloy filaments showed that high control forces could be generated.[12] Although the effectiveness of aircraft control was proven, the high power consumption resulted in almost a doubling of the power supply weight.

A different approach to roll control, rather than by rigid body deflections, is achieved by using compliant materials in a deforming wing structures. This can be done by active camber control, torsional control or a change in leading edge geometry.[13] Although these approaches were proven effective for membrane wings, they are difficult to apply to wings with a significant thickness. Much higher control forces would be required, not only to sustain the aerodynamic loads but also to overcome the inherent stiffness of the structure. Using a conventional structure of ribs and spars would require relatively heavy and bulky actuators to provide these large control forces.

However, rather than wasting energy on straining a passive structure, a highly compliant structure could be designed which allows for wing deformation. On the other hand, this structure should still employ enough structural stiffness to sustain the aerodynamic loads and protect the wing from undesired aeroelastic effects (e.g. flutter and divergence).

A new approach to adaptive structures was needed to combine the advantages of the large deflections of shape memory alloy with the speed and efficiency of piezoelectric materials, while keeping costs minimized. In the past a whole range of amplification schemes were designed to increase the amount of deflection of piezoelectric actuators.[14] However, by increasing the amount of deflection, the control force decreased with a similar amount, generally resulting in a loss of total work and often a substantial weight penalty. Accordingly, a simple mechanism was required that amplified both deflection and force at the same time, while keeping complexity and costs minimized.

In an effort to satisfy these requirements a new class of piezoelectric actuators was conceived employing Post-Buckled Precompressed elements.[15–17] The governing equation for conventional piezoelectric actuators boiled down to $F_{piezo} = K\Delta x$, where a relatively small F_{piezo} fought a relatively high K to introduce a deflec-

tion, Δx. This new type of actuators followed an entirely different scheme: $F_{piezo} = (K - K_{sp})\Delta x$, where K_{sp} represented a negative spring rate mechanism. As K_{sp} approached K the amount of deflection, Δx, introduced by the same F_{piezo} could be substantially increased. It were these principles that made the new actuator applicable in wings with a substantial thickness to induce structural deformation for flight control.

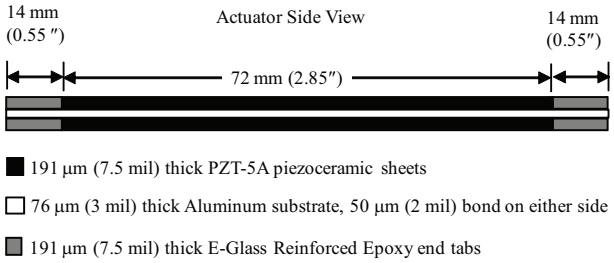

Fig. 1 Typical Lay-up of Piezoelectric Bender Actuator.

2 Analytic Model

A piezoelectric material generates a mechanical motion or a change in stress field when exposed to an electric field. Conversely they undergo a change in electric charge state when exposed to a directional change in motion or a stress field. If a positive voltage is applied to a piezoelectric material, it will lengthen in the plane perpendicularly to the axis along which the voltage was applied. If a negative voltage is applied, it will contract in the same plane. Elongations and contraction produced in this manner are very small. These longitudinal motions can be used in a bimorph configuration wherein two sheets of piezoceramic material are bonded on opposite sides of a (usually metallic) substrate (see Figure 2). When one face lengthens, the opposing face shortens and the entire assembly bends towards the shortened face. Simply reversing the voltage induces a curvature in the opposite direction. The most common piezoelectric material is the ceramic Lead Zirconate Titanate, also termed PZT. This compound exhibits greater sensitivity and higher operating temperatures than alternative piezoelectric materials.[14]

As was shown by Lesieutre, by applying a compressive force to a piezoelectric bender element, the conversion efficiency from electrical energy to mechanical work can be higher for the structure than the conversion efficiency of the material itself.[1819] To take advantage of the high deflections of the PBP actuator, a bender element was arranged in a cantilevered configuration with an external axial load applied at the tip of the actuator. Care was taken to prevent the convex actuator surface from various forms of tensile failure, including depoling and mechanical fracture. Figure 2 shows the generic cantilevered actuator arrangement with the definition of relevant parameters.

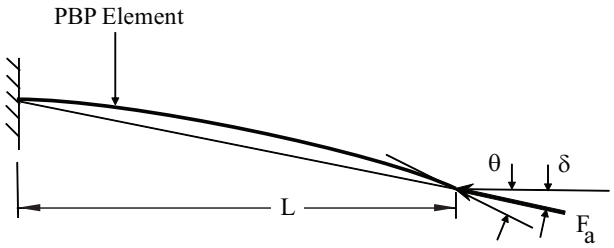

Fig. 2 Cantilevered Actuator Arrangement for the Post-Buckled Precompressed Element.

To decrease the chance of mechanical fracture in the convex actuator a classical technique was used to precompress the tension-sensitive piezoelectric elements. Cured at elevated temperatures, the mismatch in Coefficient of Thermal Expansion (CTE) induced precompression in the piezoelectric elements and pretension in the Aluminum substrates at room temperature.[20] The precompression in the piezoelectric elements ensured that even at high curvatures the convex face would still remain in compression.

The unloaded actuator actuator ($F_a = 0$) can be modeled using classical laminated plate theory (CLPT) methods.[21] Actuator in-plane forces and moments (a) are balanced by external forces and moments (ex) and forces and moments due to a mismatch in coefficients of thermal expansion (t). These forces and moments generate strains, ε, and curvatures, κ, in the laminate (l):

$$\begin{bmatrix} N \\ M \end{bmatrix}_a + \begin{bmatrix} N \\ M \end{bmatrix}_{ex} + \begin{bmatrix} N \\ M \end{bmatrix}_t = \begin{pmatrix} A & B \\ B & D \end{pmatrix}_l \begin{bmatrix} \varepsilon \\ \kappa \end{bmatrix}_l \quad (1)$$

For a bender element which is symmetric in both material properties as in geometry the amount of curvature, κ, is independent of the thermally induced stresses. The forces and moments in the laminate that are induced by the actuator elements are a function of the piezoelectric virgin strain, Λ. Assuming no external loading, equation 1 can be written as:

$$\kappa = \frac{B_a}{D_l}\Lambda \quad (2)$$

By using the unloaded curvature, κ, as a starting point, the relation between the end rotation of the actuator and the precompression force can be derived. The axial force, F_a is applied at the tip of the actuator (see Figure 2) and is directed towards the point where the actuator is cantilevered. It can be easily verified that this actuator set-up is equivalent to a pin-pin configuration of axially compressed actuators. The end rotation, θ, at the tip of of the piezoelectric actuator is related to the magnitude of the axial force. This relation is identical for both the cantilevered and the simply supported configuration:[22]

$$\theta = 2\kappa\sqrt{\frac{D_l b}{F_a}}\tan\left(\sqrt{\frac{F_a}{D_l b}}\frac{L}{2}\right) \quad (3)$$

3 Design and Production

To show how PBP actuators can be successfully applied in wings with significant thickness, a design was made for a deforming wing panel based on a NACA 0012 airfoil (see section 4.2). Two of these panels were to become the outboard stations of a 1.4m (55") subscale UAV to provide roll control. Each panel consisted of a tapered Graphite-Epoxy D-spar clamping three PBP actuators, divided over the span of the panel. The two most outboard PBP actuators measured 10mm (0.39") in width, while the center actuator measured 35mm (1,4") in width. At the trailing edge, all three actuators were connected via a thin spar composed of Aluminum, Balsa and Glass Fiber-Epoxy. The aft 70% of the airfoil was spanned by a Latex skin which was taut between the D-spar at the 30% chord and the trailing edge at the 93% chord. Figures 3 and 3 shows the design of the morphing panel.

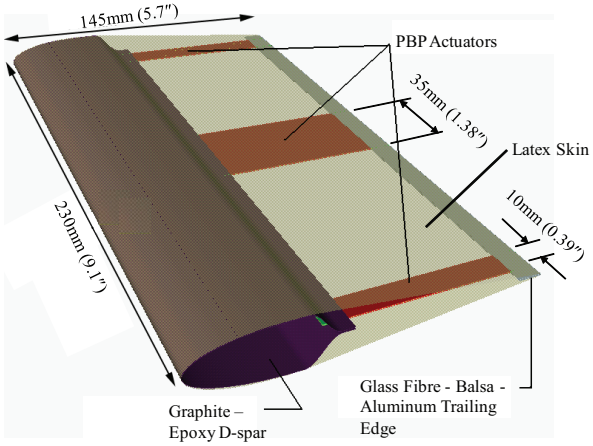

Fig. 3 Morphing Wing Section Employing PBP Actuator Elements.

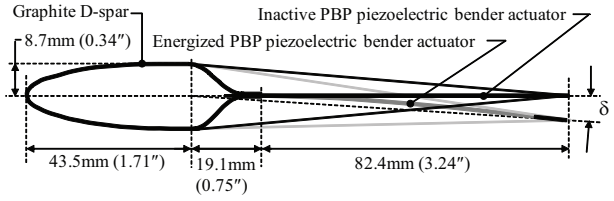

Fig. 4 Sideview of Morphing Wing Section

The latex skin fulfilled two distinct functions in this design. In the first place it acted as a highly compliant structural component which could allow for changes in camber and thickness of the profile. However, at the same time it also provided the required axial compression to the PBP actuators to increase the amount of deflection. A symmetric airfoil was chosen to have the resultant force of the upper and lower skin coincide with the plane of symmetry of the undeformed actuator elements. This ensured that the wing could change camber in the negative sense as much as in the positive sense. The force imposed

on the actuator elements by the skin resulted in an average of 70.7gmf/mm width of the actuator.

The static part of the wing consisted of a conventional balsa wood wing structure with three spars connected by ribs. To protect the actuators from over-rotating, bump stops were integrated in fences at either side of each panel. At the tips of the wing protective winglets were positioned which would protect the actuators during ground handling (see Figure 5). The wing was straight (no taper or sweep) over its entire span and exhibited a dihedral of 2 degrees. The simple structure of the morphing panel was relatively straightforward to manufacture and could easily be connected to the balsa wood wing structure. Each panel weighed in total (including wiring) 43 grams, which compared to a specific weight of 186gmf/m span. This was only a fraction higher than the specific weight of the balsa structure of the static part of the wing, which amounted to 180gmf/m span.

4 Experimental Testing and Results

4.1 Bench Testing

To determine the amplification ratio of the axially compressed actuators compared to the "free" (no compression) actuators a quasi static bench test was carried out. A signal generator in combination with a voltage amplifier introduced a sine wave signal through the piezoelectric actuators with an amplitude ranging between 0V and 100V in steps of 10V and a frequency of 1 Hz. Laser reflections off the trailing edge of the wing were projected onto a screen from which the peak-to-peak end rotations of the trailing edge could be determined within one tenth of a degree in accuracy.

Figure 4.1 shows the relation between the peak-to-peak end rotation and the voltage. The graph shows that by applying the latex skin, the end-rotations increased by more than a factor of two up to 15.8° peak-to-peak with good correlation with the analytic model up until 70V. The axially compressed elements showed a relatively high non-linearity, especially at higher voltages. Based on the maximum end rotation and the thicknesses given in Figure 2 the maximum strain on the face of the PZT elements was calculated to amount to 769μstrain. Even though it was acknowledged that the higher strains could lead to a shorter fatigue life it was not experimentally verified how the amount of end rotation decayed with number of cycles.

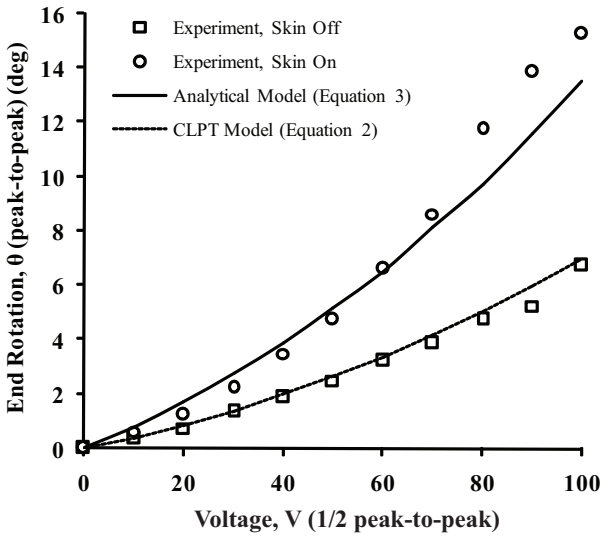

Fig. 6 Relation Between Voltage, V, and End Rotation, θ, for Skin-On and Skin-off Condition.

Complementary to the quasi-static bench test, a frequency test was carried out to find the resonance frequency for the wing with and without the latex skin applied. The same test set-up was used as for the quasi static bench test. A frequency sweep was carried out and the end rotations were recorded and normalized with respect to the quasi static end rotations.

Figure 4.1 shows that the natural frequency peak shifted from 31Hz back to 26Hz due to the application of the Latex skin. Using classical vibration theory, this suggested an increase in actuator flexibility by 30% due to the application of the skin, assuming that the skin had a negligible effect on the mass of the elements.[23] The morphing wing break frequency amounted to 34Hz, which is an order of magnitude higher than the break frequency of a conventional electromechanical servo actuator. Figure 8 shows the maximum quasi static peak to peak deflections.

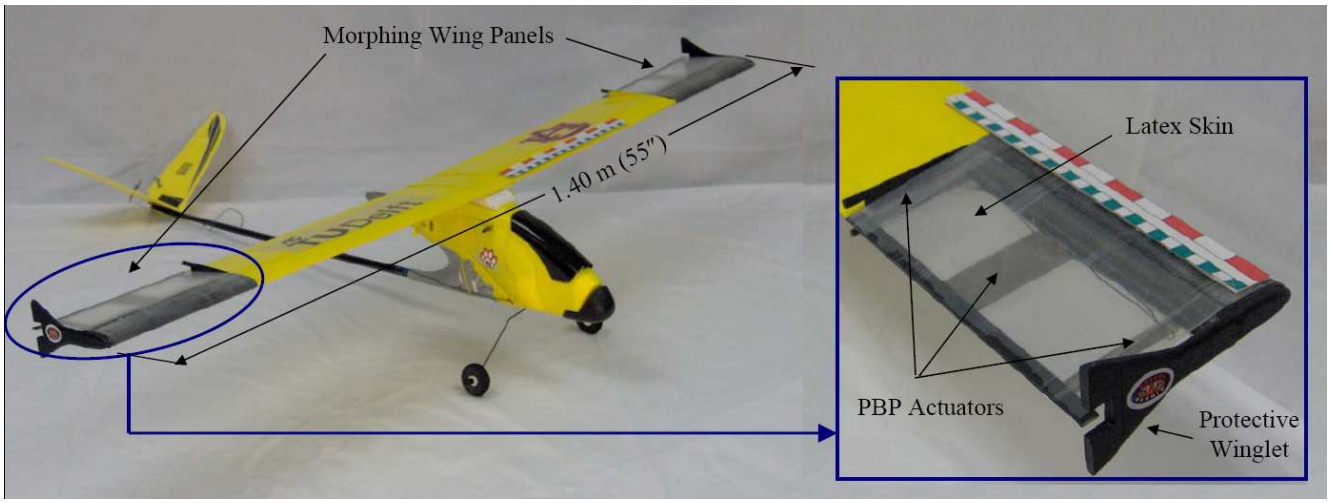

Fig. 5 UAV Employing PBP Actuated Morphing Panels

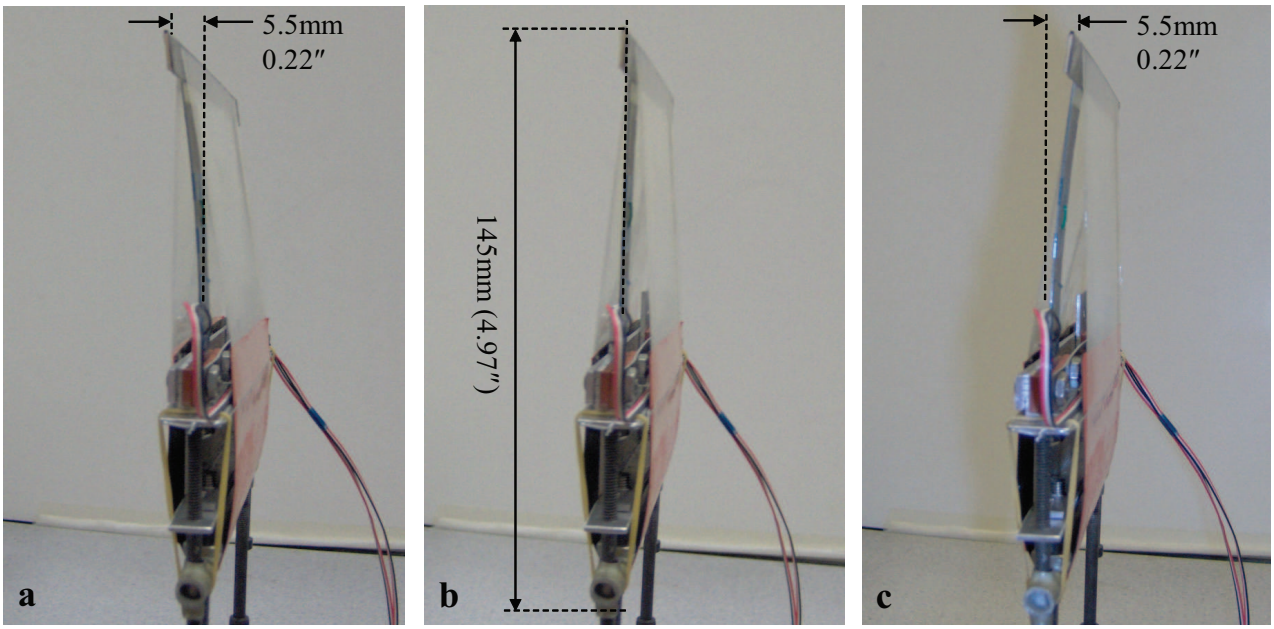

Fig. 8 Maximum Quasi Static Deflections.

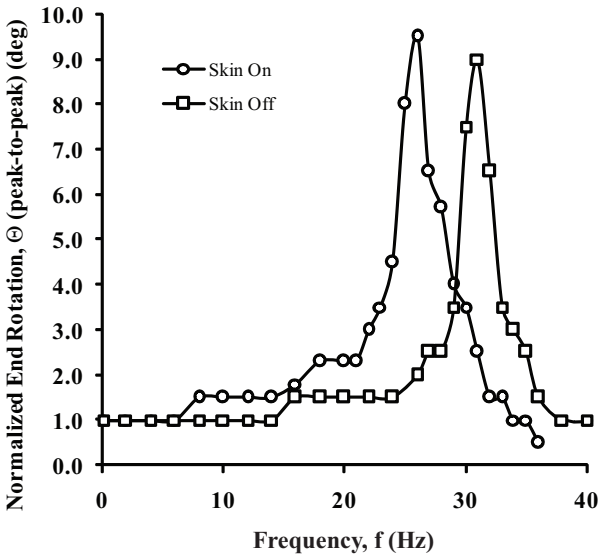

Fig. 7 Relation Between frequency, f and Normalized End Rotation, Θ, for Skin-On and Skin-off Condition.

4.2 Wind Tunnel Testing

The two-dimensional lift coefficient, c_l (not to be confused with the rolling moment coefficient, C_l) differentiated with respect to trailing-edge deflection, δ (as defined in Figure 3), is a measure for the effectiveness of a control surface. In choosing the wing section geometry for this deforming wing, a simple two-dimensional panel method (Xfoil[24])based on potential flow in combination with the Kutta condition[25] was used to predict the c_{l_δ} at various angles of attack. In order to gain as much upward as downward deflection of the morphing wing panel, a symmetric airfoil was required. The NACA 0012 airfoil was selected based on its relatively high value of c_{l_δ} at low angles of attack.

To compare the initially predicted values of c_{l_δ}, wind tunnel tests on the deforming wing panel were carried out in the Dobbinga open vertical wind tunnel at Delft University of Technology. Lift could be measured with an accuracy of 0.5 gmf (0.001lb). Lift measurements were taken at a constant wind velocity of 15 m/s. Velocity was deduced from difference in static pressure and total pressure (measured by a pitot tube in the flow). The total pressure could be measured with an accuracy of ±0.5 Pa (0.02 lb/ft^2) at a dynamic pressure of 138 Pa (2.88 lb/ft^2). The angle of attack of the wing, α, could be determined with an accuracy of ±0.05°. Figure 4.2 depicts the setup of the deforming wing panel in the open wind tunnel.

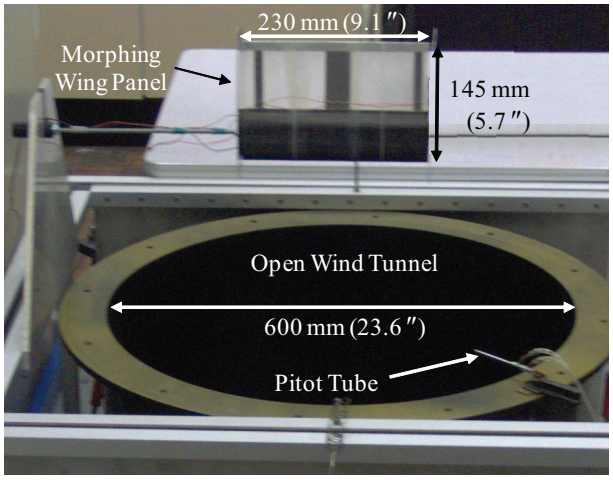

Fig. 9 Setup of Wind Tunnel Experiment in Open Wind Tunnel.

The wing was tested at four different angles of attack (α) from 0° to 15° in steps of 5°. At each position a voltage sweep was carried out from 0V to 100V in steps of 10 $(\pm 0.5^\circ)$ V. At each voltage point both lift force and deflection were recorded. From these parameters a relation is plotted between the lift coefficient, C_L, and the trailing-edge deflection, δ, in Figure 4.2.

To determine the expression for the two-dimensional lift curve slope, c_{l_δ} the reduced Polhamus equation can be used:[26]

$$c_{l_\delta} = \frac{2+\sqrt{A^2+4}}{A} C_{L_\delta}, \tag{4}$$

where A is the aspect ratio of the wing. Substituting for $A = \frac{b}{c} = \frac{230}{145} = 1.59$, and $C_{L_\delta} = 1.73\ [1/rad]$ (average value over all angles of attack) yields: $c_{l_\delta} = 4.95\ [1/rad] = 0.086\ [1/deg]$.

Table 1 shows how the measured values of c_{l_δ} compare to the results that were initially computed by Xfoil. As can be seen, the analogy between theory and experiment is limited to small angles of attack. At higher angles of attack the

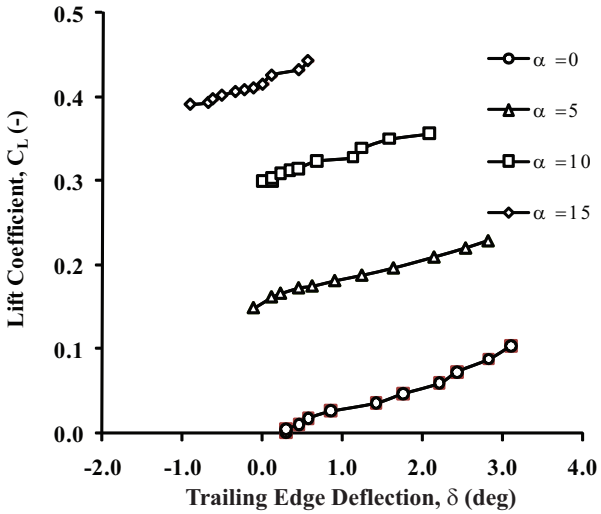

Fig. 10 Results for Wind Tunnel Test.

stall behavior of the wing could not be accurately captured by Xfoil to produce a realistic value for c_{l_δ}.

Table 1 Comparison Between Predicted and Experimental c_{l_δ}.

Angle of attack, α (deg)	Xfoil c_{l_δ} (1/rad)	Experiment c_{l_δ} (1/rad)
0	5.1	4.9
5	5.1	5.1
10	2.7	4.7
15	1.3	5.1

From Figure 4.2 it can be observed that the $C_L - \delta$ lines shift backwards at higher angles of attack. This shift is caused by the higher lift force which is applied on the actuator. This force induces an initial deflection of the actuators when no voltage is applied. Because blocked force is traded for deflection, the actuators show less deflection in opposite direction to the aerodynamic force.

4.3 Flight Testing

To show that the morphing wing panels could successfully be used to control the aircraft during flight, a flight test was conducted. The test was carried out on 29 April 2005 in Auburn, Alabama under light and variable 5 kt wind, 15deg. C (59 deg. F) and 7 statute miles of visibility. Flight test showed excellent roll control. Figure 11 shows the aircraft just after take-off. Video footage demonstrated that with respect to the baseline aircraft, the new PBP equipped aircraft had roughly 38% more roll control authority and the control derivatives were 3.7 times greater.[26]

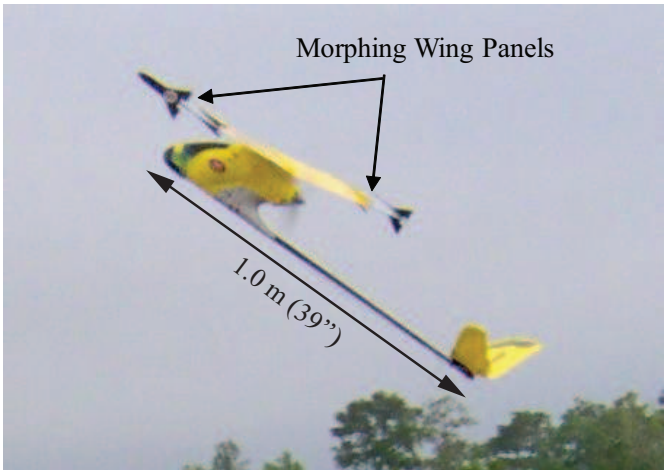

Fig. 11 Morphing Wing UAV Flight Test

5 Integration and Comparison

Significant benefits were obtained by switching from a conventional aileron actuated wing to a PBP controlled morphing wing. The morphing wing did not employ any linkages, gears, or heavy motors, and was therefore significantly lighter and less complex than a conventional wing employing ailerons controlled by electromechanical servoactuators. Due to the low complexity, it is expected that manufacturing cost of these actuators can be significantly decreased. Since the PBP actuators operated under a high voltage but very low current, power consumption was decreased substantially.[14] This in turn could lead to a reduction in battery capacity and consequently battery weight. Contradictory to conventional servo actuators, the PBP actuators were solid state, so part count, slop and deadband were one to two orders of magnitude lower.[15]

For the thick morphing wing a comparison was made between conventional electromechanical actuators controlling two ailerons on a 1.4m span UAV and the PBP actuated morphing wing panels. Table 2 shows how these two different actuators compare to each other.

Table 2 Comparison of Electromechanical Servoactuator and PBP actuator.

	Electromechanical Servo Actuator	PBP Actuator
Max. Power	$24W$	$200mW$
Max. Current	$5A$	$1.4mA$
Slop	1.6°	0.1°
Break Frequency	$3Hz$	$34Hz$
Part Count	56	6

For the thick morphing wing a weight comparison was made between the six PBP actuators that controlled the two morphing wing panels, and a high-performance sub-micro servo actuator driving two ailerons on a wing of identical size. The result of this comparison is shown in Figure 12. Because of the highly integrated actuators, no additional linkages were required and due to the low current draw, wiring could be reduced to a minimum. The comparison shows that operating empty weight could be reduced with almost 3.5% by switching from conventional aileron actuators to PBP actuated morphing wings.

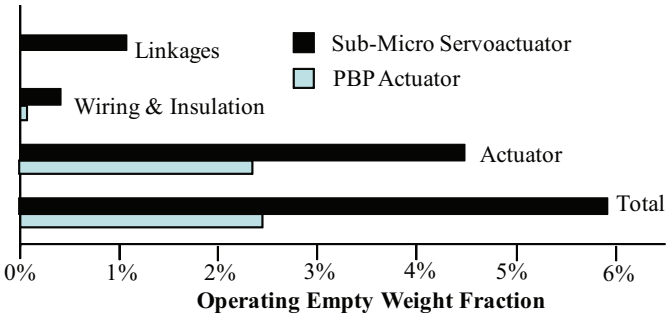

Fig. 12 Comparison of PBP and Conventional Servo Actuator Operating Empty Weight Fractions.

6 Conclusions

A synergetic design was made employing post-buckled precompressed (PBP) actuator elements in a highly compliant wing structure with significant thickness to enable roll control on a subscale uninhabited aerial vehicle (UAV). Precompression induced by a taut latex wing skin ensured an increase in end rotation of the piezoelectric actuator elements by more than 100% up to 15.8° peak-to-peak with good correlation to the analytic model. Wind tunnel tests showed that the section lift coefficient differentiated with respect to the trailing edge deflection of the wing, $c_{l_\delta} = 4.95\ [1/rad]$. Free flight tests on a 1.4 m subscale uninhabited aircraft employing morphing wing panels in place of ailerons showed roughly 38% more roll control authority and 3.7 times greater control derivatives. With respect to conventional electromechanical servo actuators, applying PBP actuators led to a saving in operating empty weight by 3.5% and an increase in break frequency from 3Hz up to 34Hz. Moreover, switching to PBP actuators decreased current draw, power consumption, slop and part count with at least an order of magnitude.

7 Acknowledgements

This research was sponsored by the Aerospace Department at Auburn University and the Faculty of Aerospace Engineering at Delft University of Technology. The author would like to acknowledge the contributions of Mr. Christoph Burger, Mr. Rick Ruysink, Mr. Leo Molenwijk, Mr. Hans Weerheim, Mr. Paolo Tiso, Mr. Roeland De Breuker, Dr. Mostafa Abdallah and Prof. Leo Veldhuis. Special thanks to Prof. Michel van Tooren and Prof. Ron Barrett for guidance throughout this project.

References

[1] Roskam, J., *Airplane Design, Part II: Preliminary Configuration Design and Integration of the Propulsion System*, DARCorp, Lawrence, Kansas, 2006.

[2] Roskam, J., *Airplane Design, Part V, Component Weight Estimation*, chap. Flight Control System Weight Estimation, DARCorp, Lawrence, Kansas, 1989.

[3] Barrett, R., *Intelligent Rotor Blade and Structures Development Using Directionally Attached Piezoelectric Crystals*, Master's thesis, University of Maryland, College Park, MD, 1990.

[4] Barrett, R., Gross, R. S., and Brozoski, F., "Missile Flight Control using Active Flexspar Actuators," *Journal of Smart Materials and Structures*, Vol. 5, No. 2, April 1996, pp. 121–128.

[5] Barrett, R., Gross, R. S., and Brozoski, F., "Design and Testing of Subsonic All-Moving Smart Flight Control Surfaces," *Procedings of the 36th AIAA Structures, Structural Dynamics and Control Conference*, AIAA Paper 95-1081, New Orleans, LA, April 1995, pp. 2289–2296.

[6] Barrett, R. and Stutts, J., "Design and Testing of a 1/12th Scale Solid State Adaptive Rotor," *Journal of Smart Materials and Structures*, Vol. 6, No. 4, August 1997, pp. 491–497.

[7] Ehlers, S. and Weisshaar, T., "Static Aeroelastic Behavior of an Adaptive Laminated Piezoelectric Composite Wing," *Proceedings of the 31st AIAA/ASME/ASCE/AHS/ASC Structures, Structural Dynamics and Materials Conference*, AIAA Paper 90-1078, Long Beach, CA, 2-4 April 1990.

[8] Ehlers, S. and Weisshaar, T., "Effect of Adaptive Material Properties on Static Aeroelastic Control," *Proceedings of the 33rd AIAA/ASME/ASCE/AHS/ASC Structures, Structural Dynamics and Materials Conference*, AIAA Paper 92-2526, Dallas, TX, 15 April 1992.

[9] Barrett, R., "Method and Apparatus for Structural Actuation and Sensing in a Desired Direction," U. S. Patent 5,440,193, August 1995.

[10] Barrett, R., "Active Plate and wing research using EDAP elements," *Journal of Smart Materials and Structures*, Vol. 1, June 1992, pp. 214–226.

[11] Barrett, R., "Adaptive Aerostructures - The First Decade of Flight on Uninhabited Aerospace Systems," *proceedings of the Society of Photo-Optical Instrumentation Engineers* 11^{th} *Annual International Symposium on Smart Structures and Materials*, Vol. 5388, 2004.

[12] Barrett, R., Burger, C., and Melian, J., "Recent Advances in Uninhabited Aerial Vehicle (UAV) Flight Control with Adaptive Aerostructures," *Proceedings of the 2001 Conference on Smart Technology Demonstrators and Devices*, Institute of Physics Publishing, Bristol and Philadelphia, June 2002, pp. 1–11.

[13] Garcia, H., Abdulrahim, M., and Lind, R., "Roll Control for a Micro Air Vehicle using Active Wing Morphing," *Proceedings of AIAA Guidance, Navigation, and Control Conference and Exhibit*, AIAA Paper 2003-5347, Austin, TX, 11-14 August 2003.

[14] Bramlette, R. and Leurck, R., "A method for control surface deflection utilizing Piezoceramic Bimorph Actuators," *Proceedings of the* 44*th AIAA Aerospace Sciences Meeting and Exhibit*, AIAA Paper 2006-146, Reno, NV, 9-12 January 2006.

[15] Barrett, R., McMurtry, R., Vos, R., Tiso, P., and DeBreuker, R., "Post-buckled precompressed (PBP) elements: a new class of flight control actuators enhancing high speed autonomous VTOL MAVs," *Proceedings of SPIE Smart Structures and Materials*, Vol. 5762, Society of Photo-Optical Instrumentation Engineers, Bellingham, WA, May 2005, pp. 111–122.

[16] Barrett, R. and Tiso, P., "PBP Adaptive Actuator Device and Embodiments," International Patent Number: PCT/NL2005/000054 by Delft University of Technology, 18 Febrary 2005.

[17] Barrett, R., Vos, R., Tiso, P., and DeBreuker, R., "Post-Buckled Precompressed (PBP) Actuators: Enhancing VTOL Autonomous High Speed MAVs," *Proceedings of the 46th AIAA/ASME/ASCE/AHS/ASC Structures, Structural Dynamics and Materials Conference*, AIAA Paper 2005-2113, Austin, TX, 18-21 April 2005.

[18] Lesieutre, G. and Davis, C., "Can a Coupling Coefficient of a Piezoelectric Device be Higher Than Those of Its Active Material?" *Journal of Intelligent Materials Systems and Structures*, Vol. 8, No. 10, 1997, pp. 859–867.

[19] Lesieutre, G. and Davis, C., "Transfer having a coupling coefficient higher than its active mate-

rial," U. S. Patent 6,236,143, May 2001.

[20] Barrett, R. M. and Stutts, J. C., "Development of a piezoceramic flight control surface actuator for highly compressed munitions," *Proceedings of the* 39^{th} *AIAA/ASME/ASCE/AHS/ASC Structures, Structural Dynamics, and Materials Conference*, AIAA Paper 98-2034, Long Beach, CA, April 20-23 1998.

[21] Jones, R., *Mechanics of Composite Materials*, chap. Micromechanical Behavior of a Lamina, Hemisphere Publishing Cooporation, fourth si ed., 1975.

[22] Vos, R. and Barrett, R., "Magnification of Work Output in PBP Class Actuators Using Buckling/Converse Buckling Techniques," *Proceedings of the 49th AIAA/ASME/ASCE/AHS/ASC Structures, Structural Dynamics and Materials Conference*, AIAA Paper no. 2008-1705, Schaumburg, IL, 7-10 April 2008.

[23] Inman, D. J., *Engineering Vibration*, Prentice-Hall, Inc., Upper Saddle River, NJ, 2nd ed., 2001.

[24] Drela, M. and Youngren, H., *XFOIL 6.94 User Guide*, MIT and Aerocraft, Inc., December 2001.

[25] Anderson, J., *Fundamentals of Aerodynamics*, McGraw Hill, 2nd ed., 1991.

[26] Roskam, J., *Airplane Design, part VI: Preliminary caluculation aerodynamic, thrust and power characteristics*, chap. Stability, control and hinge moment derivatives, DARCorp, Lawrence, Kansas, 1990.